

Dispersed Uniform Nanoparticles from a Macroscopic Organosilica Powder

Tamara L. Church,[†] Diana Bernin,^{†,‡} Alfonso E. Garcia-Bennett,[§] and Niklas Hedin^{*,†}

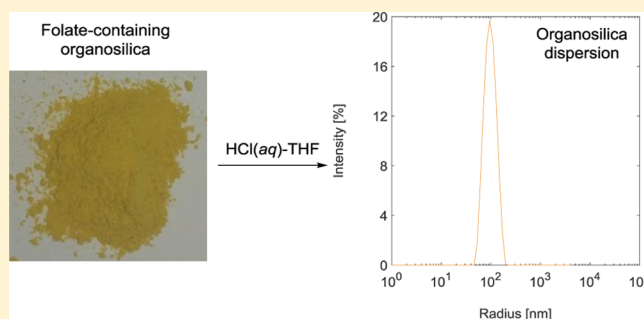
[†]Materials and Environmental Chemistry, Stockholm University, SE-106 91 Stockholm, Sweden

[‡]Swedish NMR Centre, University of Gothenburg, Box 465, SE-405 30 Göteborg, Sweden

[§]Department of Chemistry and Biomolecular Sciences, Australian Research Council Centre for Nanoscale Biophotonics, Macquarie University, Sydney, New South Wales 2109, Australia

Supporting Information

ABSTRACT: A colloidal dispersion of uniform organosilica nanoparticles could be produced via the disassembly of the non-surfactant-templated organosilica powder nanostructured folate material (NFM-1). This unusual reaction pathway was available because the folate and silica-containing moieties in NFM-1 are held together by noncovalent interactions. No precipitation was observed from the colloidal dispersion after a week, though particle growth occurred at a solvent-dependent rate that could be described by the Lifshitz–Slyozov–Wagner equation. An organosilica film that was prepared from the colloidal dispersion adsorbed folate-binding protein from solution but adsorbed ions from a phosphate-buffered saline solution to a larger degree. To our knowledge, this is the first instance of a colloidal dispersion of organosilica nanoparticles being derived from a macroscopic material rather than from molecular precursors.



INTRODUCTION

Hybrid materials of nanostructured silica, organosilica, and organics can be used as precursors for porous materials or as vehicles for a controlled delivery of molecules and display useful optical and electronic properties.^{1,2} The internal structures of such hybrid materials can be tuned by varying the fractions of their components as well as by moderating the intermolecular interactions among the components during the formation of the hybrid material. We have synthesized and studied the NFM-1 family of such hybrid materials, which consists of silica and positively charged organosilica interacting with microphase-separated organic domains of stacked Hooqsteen-bonded tetrads of folate.^{3,4} Folate is a B-vitamin (B9) and is relevant to the detection and targeting of nanoparticles toward cancer cells.^{5,6} The hybrid organosilica materials based upon folate could be transformed into nanoporous solids by removing the organic fractions via combustion or extraction. Related synthetic approaches have also been used to prepare organosilica hybrid materials based upon guanosine monophosphate.^{7,8}

Nanoparticles of silica, mesoporous silica, organosilica, and various hybrid materials are also relevant to applications in biomedicine and other fields.^{9–11} Their nanoscopic dimension allows them to be dispersed in solvents and to be assembled into mesoscaled structures, even in a crystalline manner.¹² Typically, organosilica particles are synthesized from small-molecule organosilanes, $R_xSi(OR')_{4-x}$ (R may be a bifunctional bridge or contain other functional groups), under sol–gel

conditions^{10,13} in analogy to the Stöber approach that has been quite successful in the synthesis of monodisperse nanoscale particles of silica¹⁴ and mesoporous silica.^{15,16} The nanoscale dimension is controlled via the synthetic parameters (solvents, concentration, pH, etc.).

Important to the evolution of coarsening silica and organosilica nanoparticle dispersions are, among other things, the interparticle interactions and the concentration of the nanoparticles. The former are typically described by the Derjaguin–Landau–Verwey–Overbeek (DLVO) theory, and the extent of the repulsive contributions will effectively control the aggregation tendencies.¹⁷ Nevertheless, the stability of silica particle dispersions in particular is often larger than what the DLVO theory would predict.¹⁸ In the case of Ostwald ripening, the solubility and diffusivity of the chemical entities constituting the nanoparticles dictate the evolution of particle size.^{19,20} The synthesis and specifics of the colloidal stability of monodisperse particles of silica and organosilica (based on condensed aminopropyltriethoxysilane) have been studied by van Blaaderen and Vrij.²¹ They showed that $Si(OEt)_4$ and $H_2N(CH_2)_3Si(OEt)_3$, when combined with an ammonia catalyst, formed organosilica particles. Aminoalkyl-substituted Si atoms were present throughout the particles, rather than

Received: October 24, 2017

Revised: January 15, 2018

Published: February 5, 2018

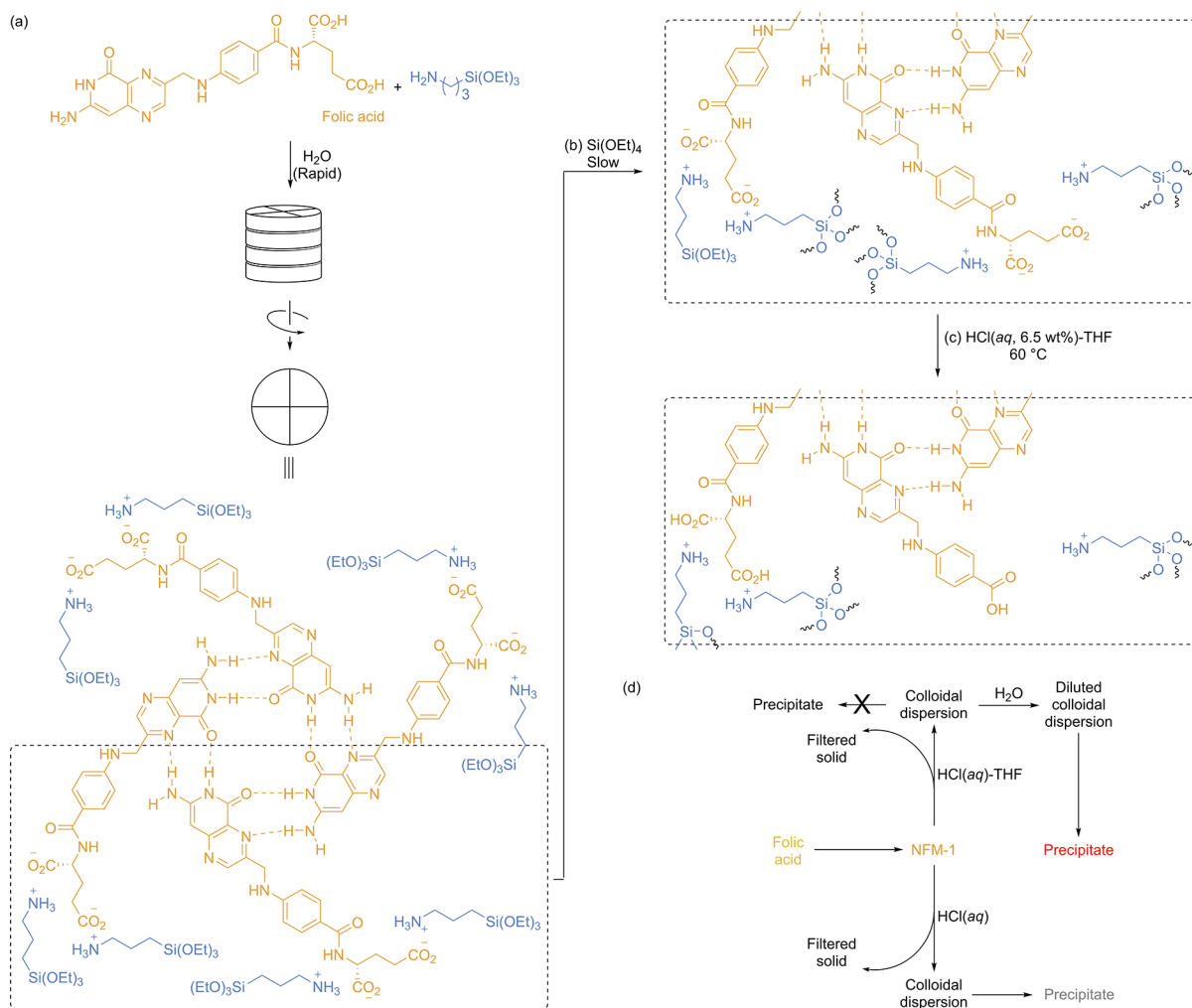


Figure 1. The synthesis of NFM-1 and colloidal dispersions derived from NFM-1 in $\text{HCl}(\text{aq})$ -THF. (a) Stacks of folate tetramers with $\text{H}_3\text{N}^+(\text{CH}_2)_3\text{Si}(\text{OEt})_3$ counterions are formed quickly upon the deprotonation of folic acid in water that contains $\text{H}_2\text{N}(\text{CH}_2)_3\text{Si}(\text{OEt})_3$. (b) Over a period of hours, the ethoxysilane groups of $\text{H}_3\text{N}^+(\text{CH}_2)_3\text{Si}(\text{OEt})_3$ and $\text{Si}(\text{OEt})_4$ are hydrolyzed and condensed to form siloxane bonds. (c) Heating the material in 11:9 v/v $\text{HCl}(\text{aq}, 6.5 \text{ wt } \%)$ -THF hydrolyzes some folic acid moieties to pteric acid. The carboxylic acids are protonated under these conditions. (d) Graphical summary of the dispersion of NFM-1.

simply forming a layer on their surfaces, and the particles were less dense than expected for analogous silica particles.

Extending these studies, we here present a solution-based method to treat macroscopic powder of the mesostructured organic-organosilica-silica hybrid NFM-1 (Figure 1) to give a suspended silica-rich solid and dispersed nanoparticles; this constitutes the first synthesis of dispersed organosilica nanoparticles from a macroscopic organosilica material. The chemical composition and the stability of the dispersed nanoparticles were studied, as was the use of thin films derived from the coarsening dispersion in the microgravimetric detection of folate-binding protein (FBP).

RESULTS AND DISCUSSION

The nanostructured composite NFM-1 was synthesized from folic acid, $\text{Si}(\text{OEt})_4$, and $\text{H}_2\text{N}(\text{CH}_2)_3\text{Si}(\text{OEt})_3$ in water.³ To understand how this yellow organosilica powder could be dispersed as nanoparticles, we briefly discuss the mechanism of its formation, which Atluri et al. have examined using X-ray diffraction (XRD), small-angle X-ray scattering, and conductivity measurements.⁴ Folic acid is poorly soluble in H_2O but dissolves upon the deprotonation of its glutamate moieties

in base.²² Thus, when a mixture of $\text{Si}(\text{OEt})_4$ and $\text{H}_2\text{N}(\text{CH}_2)_3\text{Si}(\text{OEt})_3$ (both in excess relative to folic acid) is added to a suspension of folic acid in H_2O , some of the amines are protonated, yielding $\text{H}_3\text{N}^+(\text{CH}_2)_3\text{Si}(\text{OEt})_3$ and water-soluble folate ions. Aqueous folates associate into columns of stacked hydrogen-bonded tetramers, with the aromatic pterin-based moieties inside the columns and the charged glutamate residues on the outside (Figure 1a).^{23,24} During the synthesis of NFM-1, this process takes minutes. The positively charged $\text{H}_3\text{N}^+(\text{CH}_2)_3\text{Si}(\text{OEt})_3$ ions are electrostatically attracted to the folate stacks and are therefore concentrated around them. In slower processes, the $-\text{SiOEt}$ moieties from the protonated $\text{H}_3\text{N}^+(\text{CH}_2)_3\text{Si}(\text{OEt})_3$ ions, as well as from $\text{Si}(\text{OEt})_4$ and $\text{H}_2\text{N}(\text{CH}_2)_3\text{Si}(\text{OEt})_3$, are hydrolyzed to give $\equiv\text{SiOH}$ groups that subsequently condense to form siloxane bonds (Figure 1b). The result is a composite material in which folate tetramer stacks are arranged in a hexagonal lattice, with the glutamate moieties of the folates being associated with ammonium groups that are in turn connected via alkyl groups to an organosilica-silica hybrid; the degrees of alkoxy silane hydrolysis and silica condensation, and therefore the relative fractions of organosilica and silica, depend upon postsynthetic treatment.⁴ The

NFM-1 composite synthesized and studied here was not subjected to postsynthesis hydrothermal or calcination treatments, and as a result, the silica portion of the material was not very highly condensed; single-pulse and quantitative solid-state ^{29}Si NMR spectroscopy (Figure S1) revealed that approximately 55% of the Q sites (Si atoms connected to four O atoms²⁵) were fully condensed Q⁴ sites. Alkylated Si atoms (i.e., those bearing $-\text{propylamine}$ or $-\text{propylammonium}$ chains; T sites²⁵) made up 49% of the Si atoms in the sample (cf. 24% in a hydrothermally treated sample³). By mass, NFM-1 was primarily composed of an organic material and condensable hydroxyl groups, as only 32% of its mass remained after combustion to 850 °C in air (thermogravimetric analysis, TGA; Figure S2). Nevertheless, the powder XRD pattern of NFM-1 (Figure S3) displayed sharp peaks evincing the stacking of folic acid tetramers and the existence of a mesoscale hexagonal lattice,⁴ as well as the broad wide-angle X-ray scattering peak associated with amorphous SiO_2 . The IR spectrum of NFM-1 (Figures 4 and S4) was consistent with the one reported,⁴ and the solid was also fluorescent, displaying emission spectra similar to those of folic acid (Figure S5).

Hydrothermally treated NFM-1 (NFM-1-h) can be heated at 60 °C overnight in $\text{HCl}-\text{EtOH}$ to give a white solid,⁴ indicating the removal of the folic acid component. On the other hand, we recently observed that treating the as-synthesized NFM-1 with $\text{HCl}(\text{aq})$ and THF yielded a near-homogeneous suspension. Thus, heating NFM-1 in a mixture of 11:9 v/v $\text{HCl}(\text{aq}, 6.5 \text{ wt } \%)$ and THF (this mixture is hereafter denoted “ $\text{HCl}(\text{aq})-\text{THF}$ ”) for 2 h at 60 °C produced a mixture from which only a small amount of solid could be filtered. Here, the term “suspension” refers to the mixture prior to filtration and “dispersion” to the clear bright yellow filtrate. The IR spectrum of the very pale yellow filtered solid (Figures 2 and S4) showed it to be primarily silica. The solid retained some IR absorbance in the region 1700–1420 cm^{-1} , evincing organic compounds; however, these absorbance bands were significantly less intense relative to the $\nu(\text{Si}-\text{O})$ bands compared to the case of NFM-1. The solid retained 59% of its mass following combustion to 850 °C (Figure S2a), and

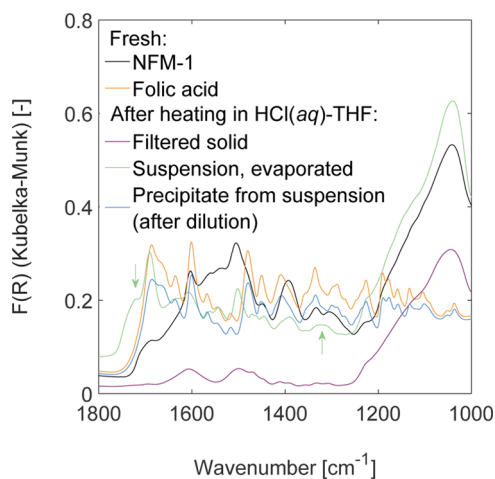


Figure 2. Attenuated total reflectance IR spectra of folic acid and NFM-1, as well as of the products of NFM-1 suspension in 11:9 v/v $\text{HCl}(\text{aq}, 6.5 \text{ wt } \%)$ –THF: the solid filtered after heating in 11:9 $\text{HCl}(\text{aq}, 6.5 \text{ wt } \%)$ –THF, the dispersion following evaporation at 0 °C, and the precipitate formed from the dispersion following 20 \times dilution in H_2O . Arrows indicate bands assigned to pteric acid.

mass loss occurred primarily between 200 and 300 °C (Figure S2b), indicating that it was mostly due to the decomposition of alkoxy- and alkylsilane groups and, potentially, to the glutamate tails of folic acid molecules.³ Unlike NFM-1, the filtered solid showed no increase in the rate of mass loss above 470 °C, indicating that it had a lower aromatic (i.e., the pterin “heads” of folic acid) content.

The bright yellow filtered dispersion that formed after heating NFM-1 in $\text{HCl}(\text{aq})-\text{THF}$ fluoresced, like aqueous folic acid,²⁶ with $\lambda_{\text{max}} = 450 \text{ nm}$ when irradiated with near-UV light (Figure S6). To investigate the chemical nature of the dispersed particles, a freshly prepared and filtered sample was cooled in an ice bath, and the solvent was removed in vacuo to give a dark yellow solid. This solid could be combusted almost completely, leaving a residue of 8.8 wt % as a white solid (Figure S2). Nevertheless, both its IR (Figures 2 and S4) and its ^{29}Si NMR (Figure S1) spectra showed that it contained silica. Further, solid-state ^{29}Si NMR revealed that the silica in the evaporated colloidal dispersion was more condensed than in NFM-1, as expected given that the heat and low pH applied in the suspension favor the condensation of silicic acid moieties.²⁷ Monoalkylated Si atoms (T sites) formed a slightly greater proportion of the Si atoms in the evaporated colloidal dispersion than in the original NFM-1 (Figure S1). This difference is consistent with a molecular structure of NFM-1 that contains silica-like domains that are not dispersed upon heating in $\text{HCl}(\text{aq})-\text{THF}$ but instead form a silica-rich precipitate that is removed by filtration. The presence of such silica-like domains is also consistent with the observation that the solid filtered from the suspension contained a greater fraction of inorganics than either NFM-1 or the evaporated colloidal dispersion (postcombustion residues of 59, 32, and 8.8 wt %, respectively, Figure S2a), as well as with both the mechanism of NFM-1 formation⁴ and the observation that calcination of NFM-1-h in air yields an ordered mesoporous silica with channels in place of the folic acid stacks.³

The IR spectrum of the evaporated colloidal dispersion derived from NFM-1 in $\text{HCl}(\text{aq})-\text{THF}$ (Figures 2 and S4) contained new bands at 1718 and 1322 cm^{-1} , consistent with pteric acid.²⁸ Thus, the amide bonds of at least some folic acid molecules were hydrolyzed during the treatment with $\text{HCl}(\text{aq})-\text{THF}$, as has been observed under more severe conditions.^{29,30} The decarboxylation of pteric acid has also been observed under acidic conditions,³⁰ and we cannot rule out its occurrence here. The hydrolysis of folic acid separates its pterin-based “heads”, which lay in the center of the organic folate stacks in NFM-1, from their glutamic acid “tails” (Figure 1c). On the basis of TGA (Figure S2), we estimate (see the Supporting Information for details) that a minimum of 26% of the folic acid was hydrolyzed, with the liberated glutamic acid likely being adsorbed on the solid that was filtered from the suspension. Glutamic acid forms hydrogen bonds with silica,^{31,32} and the adsorbed material can nucleate the formation of glutamic acid crystallites on silica;³¹ this would favor the adsorption of glutamic acid on the silica-rich solid.

The scission of folic acid molecules to give pteric acid is not necessarily required to separate a suspended silica-rich solid from the dispersion of nanoparticles containing primarily an organic matter that is formed by heating NFM-1 in $\text{HCl}(\text{aq})-\text{THF}$. The folate and silica-rich domains of NFM-1 itself are not held together by covalent bonds; rather, electrostatic and van der Waals interactions mediate the association between the folate ions and the alkylammonium-substituted Si compounds

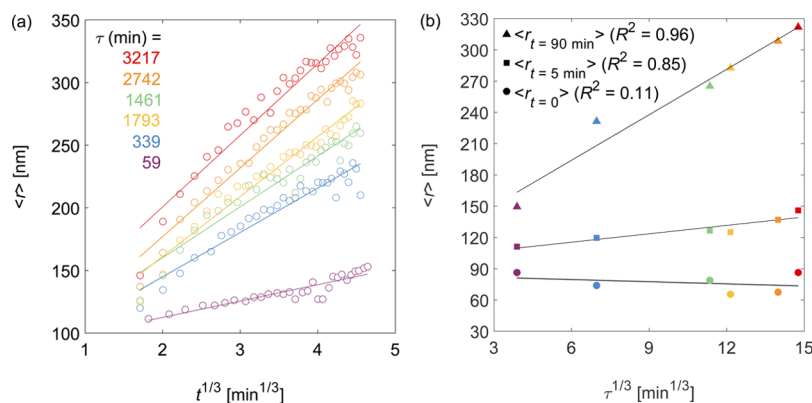


Figure 3. (a) Variation of the average radius of dispersed colloidal particles with the cube root of the time t since a dispersion of NFM-1 was diluted from HCl(aq)–THF to give dilute HCl(aq)–THF. (b) Variation of the average radius of dispersed colloidal particles with the cube root of the time τ since NFM-1 was dispersed. The values $\langle r_0 \rangle$ are the y -intercepts of the LSW plots in (a) and $\langle r_{t=5 \text{ min}} \rangle$ and $\langle r_{t=90 \text{ min}} \rangle$ are the average radii measured 5 and 90 min, respectively, after dilution, at each value of τ in (a). The color of each data point corresponds to the relevant curve in (a).

(Figure 1b). Further, the acidic medium causes nonhydrolytic changes to the NFM-1. It is formed under mildly basic conditions (pH early in the synthesis was 8.5); acidification of the solid below the pK_a values of the carboxylic acids ($pK_a = 2.155$ and 4.324 for the α - and γ -carboxylic acids, respectively, in glutamic acid³³) converts folate to folic acid. Pteric acid ($pK_a \approx 2.29$ ³⁴) is also expected to be in its acid (i.e., protonated) form at the pH of the colloidal dispersion derived from NFM-1 in HCl(aq)–THF. No sharp $\nu(\text{O–H})$ band indicating isolated $-\text{OH}$ groups was visible in the infrared spectrum of the evaporated colloidal dispersion (Figure S4), indicating that the carboxylic acids interacted with other species; nevertheless, changes in the protonation states of various species in the solid could be important in disrupting the interactions that hold the organic and inorganic portions of NFM-1 together. As mentioned, folic acid has been removed from hydrothermally treated NFM-1-h by heating in HCl–EtOH.^{3,4} In contrast, we observed here that heating NFM-1 in HCl(aq)–THF did not simply remove folic acid from the composite, as the dispersion also included inorganics. To better understand the contents of the dispersion and the factors influencing its formation, we examined the colloidal dispersion derived from NFM-1 in HCl(aq)–THF immediately after filtering.

Although the filtrate formed by dispersing NFM-1 in HCl(aq)–THF appeared homogeneous to the naked eye, dynamic light scattering (DLS) revealed dispersed colloidal particles. As the initial colloidal dispersion had a concentration close to 5 mg/mL and was prepared in a solvent mixture, it was diluted 20 \times in deionized H₂O to give a more dilute sample in a primarily aqueous medium for DLS measurements; the diluted dispersion was 391:9 v/v HCl(aq, 0.33 wt %)-THF and is hereafter labelled “dilute HCl(aq)–THF”. The diluted dispersion contained nanoparticles whose average initial radius was ~ 90 nm (Figure 3), with a low polydispersity index (PDI) of ~ 0.15 (Figure S7a). The nanoparticles were therefore more than an order of magnitude larger than the hexagonal unit cell in NFM-1⁴ or than the length or width of a single folate stack in H₂O.^{23,35} They were only slightly larger than the nanoparticles formed when folic acid alone was dispersed in HCl(aq)–THF for 2 h at 60 °C (initial radius ≈ 80 nm, PDI ≈ 0.06 ; see Figure S8). On the basis of their size and content, the particles are expected to be made up of columns of folic/ptericoic acid tetramers intermingled with domains of moderately condensed

alkyl- and alkoxy-silanes. The powder XRD pattern of the evaporated dispersion (Figure S3) indicates that some long-range order is maintained in these particles. The order was also evident in some particles observed in transmission electron microscope images of evaporated dispersion (Figure S9).

The time evolution of the average radius $\langle r \rangle$ of the particles dispersed from NFM-1 could be described by the Lifshitz–Slyozov–Wagner (LSW) equation^{19,20,36} (Figure 3). Plots of $\langle r \rangle$ versus the cube root of time were linear for two timescales, each relevant to a different medium. Here, τ is the time elapsed since the NFM-1 was dispersed in HCl(aq)–THF, and t is the time elapsed since the sample was diluted in deionized H₂O for DLS. The particle radii maintained a low PDI throughout (Figure S7). Ackerson and co-workers³⁷ and Penders and Vrij³⁸ observed that the average radii of particles in destabilized dispersions of stearyl-functionalized silica in benzene also grew with the cube root of time, at least after the initial 20–30 s. The adherence of the ripening of NFM-1 particles dispersed in dilute HCl(aq)–THF to the LSW equation (i.e., the dependence of $\langle r \rangle$ on the cube root of t) suggests that our system is steered by physics similar to that applicable in the systems of Ackerson and co-workers³⁷ and Penders and Vrij.³⁸ In diluted and coarsening dispersions of NFM-1, the apparent LSW slopes for particle growth after dilution increased with τ (Figure 3a). The dependence of $\langle r \rangle$ on τ was evaluated in two ways. First, the earliest data point measured following each dilution (i.e., $\langle r_{t=5 \text{ min}} \rangle$ for each τ) was linearly correlated with $\tau^{1/3}$ ($R^2 = 0.85$). The same was true a longer time after dilution; for example, $\langle r_{t=90 \text{ min}} \rangle$ was also linearly correlated with $\tau^{1/3}$ ($R^2 = 0.96$). Alternatively, the intercept $\langle r_0 \rangle$ of the LSW plot for a diluted and coarsening colloidal dispersion (Figure 3a) could be used as a proxy for the aggregation of particles in the undiluted dispersion. However, $\langle r_0 \rangle$ was poorly linearly correlated with $\tau^{1/3}$ ($R^2 = 0.11$, Figure 3b). The much better correlation of $\langle r \rangle$ versus $\tau^{1/3}$ when the former is measured after, for example, $t = 5$ min, rather than extrapolated to $t = 0$ for each dilution suggests that the particle growth may not exhibit the LSW behavior immediately after dilution, which would also be consistent with the observations of Ackerson and co-workers³⁷ and Penders and Vrij.³⁸

The $\langle r \rangle$ increased more rapidly with t than with τ ; the slopes of the LSW plots of $\langle r \rangle$ versus $t^{1/3}$ (Figure 3a) were 5–20 \times greater than the one for the plot of $\langle r_{t=5 \text{ min}} \rangle$ versus $\tau^{1/3}$ (Figure 3b). Therefore, the particles ripened more rapidly in the diluted

391:9 v/v HCl(aq, 0.33 wt %)-THF medium than in the initial 11:9 v/v HCl(aq, 6.5 wt %)-THF. Considering the LSW description of particle ripening in dispersion and assuming that the molar volume of the dispersed material is independent of solvent, the different LSW slopes with respect to t and τ must be related to changes in the surface energies, solubilities, and diffusivities of the subparticles or constituent molecular entities. The relevant diffusion coefficients are not known, but the ratio of viscosities of the initial and diluted solvent mixtures (i.e. without contributions from the particles themselves) can be estimated as $\sim 2:1$ (see the Supporting Information for details). In this analysis, differences in surface energies and solubilities contribute to a 3–10 \times greater rate of ripening in the diluted colloidal dispersion. The low pH of the matrix produced a small positive surface charge on the particles (a diluted sample with $t = 2$ min and $\tau = 300$ min had ζ -potential of +17 mV), and the differences in particle growth in the initial and diluted dispersions can therefore also be rationalized in terms of screening potential and interparticle interactions. We speculate that the primarily aqueous dilute HCl(aq)-THF matrix provided greater electrostatic screening than the initial HCl(aq)-THF mixture and thus better facilitated particle growth. This effect would however be mitigated by the greater concentration of dissolved ions (i.e., HCl(aq)) in the undiluted dispersion. A particle dispersion prepared from NFM-1 in more concentrated HCl(aq), that is, HCl(aq, 11.2 wt %)-THF, and then diluted for measurement, contained polydisperse particles.

The concentration of THF in the medium not only decreased the rate of particle growth in the dispersion derived from NFM-1 but was also decisive in the rate of sedimentation. The colloidal dispersion formed upon heating NFM-1 in HCl(aq)-THF for 2 h at 60 °C and subsequent filtration could be left to stand at room temperature for at least a week, and no turbidity or precipitation was observed. When this same dispersion was diluted 20 \times in H₂O to give dilute HCl(aq)-THF, folic acid precipitated (IR spectrum Figures 2 and S10, powder XRD pattern Figure S11). THF did not have to be present during the heating phase though; heating NFM-1 in HCl(aq, 6.5 wt %) for 2 h at 60 °C, then adding THF after cooling but before filtration, also yielded a dispersion of nanoparticles from which no precipitation was observed after a week. A DLS sample prepared by dilution of this mixture showed $\langle r \rangle \approx 45$ nm with PDI ≈ 0.13 (Figure S12). On the other hand, a dispersion formed by heating NFM-1 in only HCl(aq, 6.5 wt %), then filtering the resulting mixture, also gave a filtrate that appeared homogeneous to the naked eye, but DLS measurements of this dispersion following dilution showed it to contain polydisperse particles whose sizes ranged from the nm to μ m scales. In less than 24 h, a yellow solid composed primarily of organic compounds (see the IR spectrum Figure S10) precipitated from the undiluted HCl(aq, 6.5 wt %) filtrate.

To test the hypothesis that the lower polarity (and thus screening potential) of THF compared to that of H₂O stabilized the organosilica dispersion by slowing particle aggregation, we repeated the decomposition of NFM-1 in a mixture of aqueous acid and 1,4-dioxane, a cyclic dialkyl ether that is less polar than THF. Thus, NFM-1 was heated in 11:9 HCl(aq, 6.5 wt %)-1,4-dioxane (hereafter labelled "HCl(aq)-dioxane") for 2 h at 60 °C, then filtered to give a yellow dispersion. DLS measurements demonstrated that a diluted colloidal dispersion contained smaller particles than those dispersed in HCl(aq)-THF (Figure 4). Particle ripening

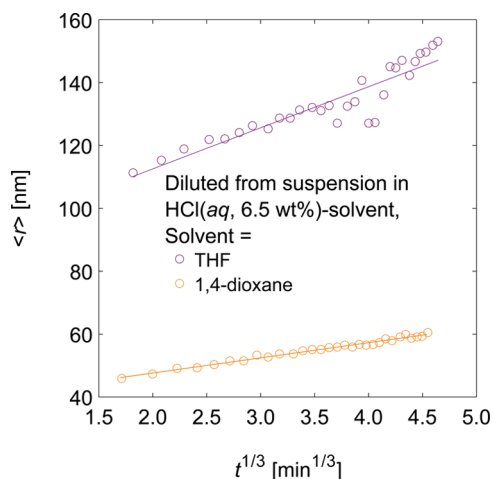


Figure 4. Variation of the radius of dispersed particles with the cube root of the time t elapsed since a freshly dispersed and filtered dispersion of NFM-1 in an HCl(aq)-solvent mixture was diluted in deionized H₂O.

occurred more slowly in the diluted mixture containing 1,4-dioxane than in the one containing THF, and particle growth in the undiluted HCl(aq)-dioxane dispersion was too slow to be reliably evaluated. These observations support the hypothesis that the ether co-solvent contributes to the stability of the dispersion by poorly shielding electrostatic repulsion between the positively charged surfaces of the organosilica particles. Alternatively, or possibly consistent with the LSW-based explanation, the differences in the behavior of the nanoparticles in the diluted THF- and dioxane-containing dispersions could relate to changes in the surface energies, solubilities and diffusivities of subparticles or constituent molecular entities.

Thermogravimetric and IR spectroscopic data indicated that the colloidal dispersion produced by heating NFM-1 in HCl(aq)-THF contained primarily not only folic and pteric acids but also silica and organosilica, and we therefore investigated the possibility that films could be formed from the coarsening dispersion derived from NFM-1. The generation of thin films from colloidal suspensions has several advantages over other methods, with technical simplicity and the ability to control microstructure being especially important.³⁹ Thin films formed from suspensions of silica nanoparticles in particular have been used, for example, as antireflective coatings⁴⁰ and to encourage the growth of cells on surfaces.⁴¹ Films containing folic acid have proven useful for the detection of a 5-methylcytosine-genomic content (i.e., DNA from cancer cells),⁴² cancer cells,^{43,44} and FBP (which is overexpressed in multiple types of tumor cells).⁴⁵ A cracked film (Figure S13) could be obtained by placing a few drops of dispersion on a glass substrate and allowing it to dry, indicating that film formation was possible, and we therefore attempted to deposit a thin film of dispersed NFM-1 on a Au sensor. Savran and co-workers have reported a folate-modified sensor that, when monitored in a quartz crystal microbalance (QCM), could be used to detect as little as 30 nM FBP, and this detection limit could be lowered to 50 pM FBP following additional modifications of the sensor.⁴⁵ Thus, a diluted dispersion of NFM-1 was spin-coated onto on an Au sensor (see the Supporting Information for details). Regions of yellow color that were distinct from the Au sensor were visible near the outside of the coated sensor. An IR spectrum of a yellow region

was recorded on an IR microscope, as was a spectrum of a region on which only the sensor was visible, and both contained $\nu(\text{Si-O})$, $\nu(\text{O-H})$ and $\nu(\text{C-H})$ bands (Figure S14), suggesting the film derived from NFM-1 covered the sensor even when it was not visible in the microscope. The IR spectra also displayed interference, a characteristic of thin-film samples.⁴⁶

The response of the NFM-1-derived film to aqueous solutions of FBP was examined in a QCM apparatus with dissipation monitoring (Figure 5). The film-loaded chip did not

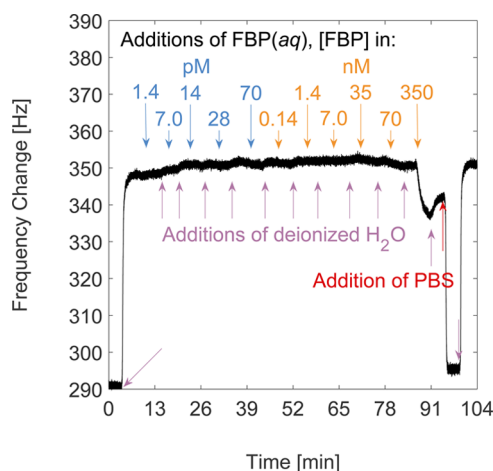


Figure 5. Frequency changes for a Au-coated quartz crystal sensor with an organosilica film deposited from a diluted dispersion of NFM-1 upon exposure to solutions of FBP and of PBS. Repeated flushing with H₂O was performed as indicated.

respond to pM concentrations of FBP, but very slight changes in the chip vibration frequency were observed upon exposure to 35 and 70 nM FBP solutions, and a 350 nM FBP solution produced a clear drop in the frequency of the chip. Thus, the film derived from NFM-1 did increase in mass upon exposure to FBP, presumably because of the binding of this protein to folic acid, and the chip showed a detection limit on the same order of magnitude as the sensor described by Savran and co-workers.⁴⁵ A much larger response was noted when the film-coated sensor was exposed to a phosphate-buffered saline (PBS) solution, indicating that the film readily adsorbed one or more of the Na⁺, K⁺, or H_xPO₄^{(3-x)-} ($x = 1$ or 2) ions. This response occurred regardless of whether the film had already been exposed to FBP and was reversible upon washing with deionized water. Although this marked response to aqueous salts would likely preclude the use of thin films derived from NFM-1 in the microgravimetric detection of FBP in biological fluid, it may offer further information regarding the structure of the suspended nanoparticles formed when NFM-1 is dispersed in HCl(aq)–THF. Tetramers of molecules based upon folic acid^{47,48} and the related 5'-guanosine monophosphate⁴⁹ readily accommodate Na⁺ and K⁺ ions in their central channels, which could account for some of the mass gain for the coated sensor upon exposure to the PBS. However, in further investigations (Figure S15), only a small mass change occurred when the film was exposed to NaCl(aq, 50 mM), and similar results were obtained for KCl(aq, 50 mM). A solution containing Na₂HPO₄(aq) and KH₂PO₄(aq) in the concentrations used in PBS buffer, but without NaCl or KCl, produced a larger weight change in the film, but the response to PBS buffer was

several times greater, suggesting the synergistic uptake of ions, and possibly of water, from that solution.

CONCLUSIONS

Already upon its development, NFM-1 was an unusual organosilica composite in that it was held together by multiple weak interactions between folates and protonated amino-propylsilicates rather than by covalent bonds, and it represented the synthesis of mesoporous silica via a nonsurfactant mechanism.³ We now report that, because of the interactions that adhere the microphase-separated inorganic–organic portions of NFM-1, the solid could be decomposed in a mixture of aqueous acid and an ether co-solvent such as THF or 1,4-dioxane. The result was a small amount of insoluble solid composed primarily of SiO₂, as well as a dispersion of monodisperse particles with diameters ranging from 90 to 150 nm. The particles were composed primarily of an organic material but also contained a significant inorganic fraction consisting of silica and organosilica, indicating that the folic acid was not simply washed out of the composite following the protonation of its folate groups.

The particles ripened in solution at a rate that depended on the amount and identity of the ether cosolvent. Both a larger fraction of ether in the medium and a less-polar ether solvent slowed ripening, indicating that the poor electrostatic shielding provided by the ether solvent contributed to the stability of the dispersion. Further, although some hydrolysis of folic acid to pteronic acid was observed, the suspended particles also contained intact folic acid molecules. Thus, the decomposition of NFM-1 in HCl(aq)–ether allows a macroscopic organosilica to be decomposed to form a dispersion of organosilica nanoparticles. The primary mechanism of suspension was not the breaking of covalent bonds but rather the pH-driven alterations of the weak interactions that held the material together.

Organosilica films could be derived from the dispersion and could take up FBP, although they took up more PBS.

EXPERIMENTAL SECTION

Synthesis of NFM-1. NFM-1 was synthesized according to published procedures.^{3,4} Thus, folic acid (0.680 g, 1.54 mmol) and deionized H₂O (49 mL, 2.7 mol) were combined with a magnetic stir bar in a capped jar, and the mixture was sonicated for 5 min, then allowed to stand at room temperature. Separately, tetraethyl orthosilicate (2.6 mL, 12 mmol) and 3-aminopropyltriethoxysilane (0.90 mL, 3.8 mmol) were combined in a vial. After the folic acid/H₂O mixture had stood undisturbed for 1 h, it was stirred vigorously while the silicon-containing precursors were added, and then for 30 min more. The mixture was then allowed to stand without stirring for 40 h before it was filtered through a glass frit. The yellow-orange solid was spread in a glass dish, covered with a tissue, and allowed to dry in air overnight.

Suspension of NFM-1. For suspension in a mixture of acid and THF, NFM-1 (50 mg) or folic acid was weighed into a 25 mL round-bottomed flask, and a magnetic stir bar was added. In a separate flask, concentrated hydrochloric acid (HCl(aq), 35.9 wt %, 1.0 mL, 12 mmol), deionized water (4.5 mL, 250 mmol), and tetrahydrofuran (THF, 4.5 mL, 55 mmol) were mixed to form a homogeneous liquid (denoted “HCl(aq)–THF”). This mixture was then poured into the flask containing NFM-1. The flask was fitted with a condenser and lowered into an oil bath that was held at 60 °C. After 2 h, the mixture was removed from heat and allowed to cool to room temperature, then filtered through a filter paper that retained particles having $d \geq 2 \mu\text{m}$. An analogous procedure was used to suspend NFM-1 in HCl(aq),

except that the addition of THF was omitted. Thus, only 5.5 mL solution (HCl(aq)) was added to the solid.

An analogous procedure was also used to suspend folic acid in the same medium; in that case, 17 mg folic acid was combined with 5 mL HCl(aq)-THF.

■ ASSOCIATED CONTENT

Supporting Information

The Supporting Information is available free of charge on the ACS Publications website at DOI: 10.1021/acs.langmuir.7b03705.

Full experimental details, additional characterization data for NFM-1 and its dispersion products, and estimates of viscosity and degree of folic acid hydrolysis (PDF)

■ AUTHOR INFORMATION

Corresponding Author

*E-mail: niklas.hedin@mmk.su.se.

ORCID

Diana Bernin: 0000-0002-9611-2263

Niklas Hedin: 0000-0002-7284-2974

Author Contributions

The manuscript was written through contributions of all authors. All authors have given approval to the final version of the manuscript.

Notes

The authors declare the following competing financial interest(s): Alfonso E. Garcia-Bennett is the co-founder of Nanologica AB (Stockholm, Sweden), a company commercializing nanoporous materials for biomedical and related applications.

■ ACKNOWLEDGMENTS

The authors thank the Swedish Research Council (projects #2012-3375 and 2016-03568) for support of this work. A.E.G.-B. is grateful for funding from the ARC Centre of Excellence for Nanoscale BioPhotonics (CE140100003), for an ARC Future Fellowship (AEGF, FT150100342) as well as a Macquarie University Infrastructure grant (MQRIBG9201501951). The authors thank Mathieu Meyes for laboratory support.

■ REFERENCES

- (1) Yang, P.; Wirnsberger, G.; Huang, H. C.; Cordero, S. R.; McGehee, M. D.; Scott, B.; Deng, T.; Whitesides, G. M.; Chmelka, B. F.; Buratto, S. K.; Stucky, G. D. Mirrorless Lasing from Mesoporous Silica. *Langmuir* **2013**, *29*, 12003–12012.
- (2) Yang, S.; Mirau, P. A.; Pai, C.-S.; Nalamasu, O.; Reichmanis, E.; Pai, J. C.; Obeng, Y. S.; Seputro, J.; Lin, E. K.; Lee, H.-J.; Sun, J.; Gidley, D. W. Nanoporous Ultralow Dielectric Constant Organosilicates Templated by Triblock Copolymers. *Chem. Mater.* **2002**, *14*, 369–374.
- (3) Atluri, R.; Hedin, N.; Garcia-Bennett, A. E. Nonsurfactant Supramolecular Synthesis of Ordered Mesoporous Silica. *J. Am. Chem. Soc.* **2009**, *131*, 3189–3191.
- (4) Atluri, R.; Iqbal, M. N.; Bacsik, Z.; Hedin, N.; Villaescusa, L. A.; Garcia-Bennett, A. E. Self-Assembly Mechanism of Folate-Templated Mesoporous Silica. *Langmuir* **2013**, *29*, 12003–12012.
- (5) Rosenholm, J. M.; Meinander, A.; Peuhu, E.; Niemi, R.; Eriksson, J. E.; Sahlgren, C.; Lindén, M. Targeting of Porous Hybrid Silica Nanoparticles to Cancer Cells. *ACS Nano* **2009**, *3*, 197–206.
- (6) Brigger, I.; Dubernet, C.; Couvreur, P. Nanoparticles in cancer therapy and diagnosis. *Adv. Drug Delivery Rev.* **2002**, *54*, 631–651.

- (7) Bueno-Alejo, C. J.; Villaescusa, L. A.; Garcia-Bennett, A. E. Supramolecular Transcription of Guanosine Monophosphate into Mesoporous Silica. *Angew. Chem., Int. Ed.* **2014**, *53*, 12106–12110.
- (8) Arnal-Hérault, C.; Banu, A.; Barboiu, M.; Michau, M.; van der Lee, A. Amplification and Transcription of the Dynamic Supramolecular Chirality of the Guanine Quadruplex. *Angew. Chem., Int. Ed.* **2007**, *46*, 4268–4272.
- (9) Li, Z.; Barnes, J. C.; Bosoy, A.; Stoddart, J. F.; Zink, J. I. Mesoporous silica nanoparticles in biomedical applications. *Chem. Soc. Rev.* **2012**, *41*, 2590–2605.
- (10) Croissant, J. G.; Cattoën, X.; Man, M. W. C.; Durand, J.-O.; Khashab, N. M. Syntheses and applications of periodic mesoporous organosilica nanoparticles. *Nanoscale* **2015**, *7*, 20318–20334.
- (11) Chen, Y.; Shi, J. Chemistry of Mesoporous Organosilica in Nanotechnology: Molecularly Organic–Inorganic Hybridization into Frameworks. *Adv. Mater.* **2016**, *28*, 3235–3272.
- (12) Velev, O. D.; Jede, T. A.; Lobo, R. F.; Lenhoff, A. M. Porous silica via colloidal crystallization. *Nature* **1997**, *389*, 447–448.
- (13) Nakamura, M. Biomedical applications of organosilica nanoparticles toward theranostics. *Nanotechnol. Rev.* **2012**, *1*, 469–491.
- (14) Stöber, W.; Fink, A.; Bohn, E. Controlled growth of monodisperse silica spheres in the micron size range. *J. Colloid Interface Sci.* **1968**, *26*, 62–69.
- (15) Lai, C.-Y.; Trewyn, B. G.; Jeftinija, D. M.; Jeftinija, K.; Xu, S.; Jeftinija, S.; Lin, V. S.-Y. A Mesoporous Silica Nanosphere-Based Carrier System with Chemically Removable CdS Nanoparticle Caps for Stimuli-Responsive Controlled Release of Neurotransmitters and Drug Molecules. *J. Am. Chem. Soc.* **2003**, *125*, 4451–4459.
- (16) Grün, M.; Lauer, I.; Unger, K. K. The synthesis of micrometer- and submicrometer-size spheres of ordered mesoporous oxide MCM-41. *Adv. Mater.* **1997**, *9*, 254–257.
- (17) Sigmund, W. M.; Bell, N. S.; Bergström, L. Novel Powder-Processing Methods for Advanced Ceramics. *J. Am. Ceram. Soc.* **2000**, *83*, 1557–1574.
- (18) Yotsumoto, H.; Yoon, R.-H. Application of Extended DLVO Theory. *J. Colloid Interface Sci.* **1993**, *157*, 434–441.
- (19) Lifshitz, I. M.; Slyozov, V. V. The kinetics of precipitation from supersaturated solid solutions. *J. Phys. Chem. Solids* **1961**, *19*, 35–50.
- (20) Wagner, C. Theorie der Alterung von Niederschlägen durch Umlösen (Ostwald-Reifung). *Z. Elektrochem.* **1961**, *65*, 581–591.
- (21) van Blaaderen, A.; Vrij, A. Synthesis and Characterization of Monodisperse Colloidal Organo-silica Spheres. *J. Colloid Interface Sci.* **1993**, *156*, 1–18.
- (22) Younis, I. R.; Stamatakis, M. K.; Callery, P. S.; Meyer-Stout, P. J. Influence of pH on the dissolution of folic acid supplements. *Int. J. Pharm.* **2009**, *367*, 97–102.
- (23) Bonazzi, S.; DeMorais, M. M.; Gottarelli, G.; Mariani, P.; Spada, G. P. Self-Assembly and Liquid Crystal Formation of Folic Acid Salts. *Angew. Chem., Int. Ed. Engl.* **1993**, *32*, 248–250.
- (24) Ciuchi, F.; Di Nicola, G.; Franz, H.; Gottarelli, G.; Mariani, P.; Bossi, M. G. P.; Spada, G. P. Self-Recognition and Self-Assembly of Folic Acid Salts: Columnar Liquid Crystalline Polymorphism and the Column Growth Process. *J. Am. Chem. Soc.* **1994**, *116*, 7064–7071.
- (25) Noll, W. *General Discussion A2 Chemistry and Technology of Silicones*; Academic Press, 1968; Chapter 1, pp 1–23.
- (26) Duggan, D. E.; Bowman, R. L.; Brodie, B. B.; Udenfriend, S. A spectrophotofluorometric study of compounds of biological interest. *Arch. Biochem. Biophys.* **1957**, *68*, 1–14.
- (27) Alexander, G. B. The Polymerization of Monosilicic Acid. *J. Am. Chem. Soc.* **1954**, *76*, 2094–2096.
- (28) Reference spectrum provided by Sigma-Aldrich.
- (29) Geszke, M.; Murias, M.; Balan, L.; Medjahdi, G.; Korczyński, J.; Moritz, M.; Lulek, J.; Schneider, R. Folic acid-conjugated core/shell ZnS:Mn/ZnS quantum dots as targeted probes for two photon fluorescence imaging of cancer cells. *Acta Biomater.* **2011**, *7*, 1327–1338.
- (30) Temple, C.; Rose, J. D.; Montgomery, J. A. Chemical conversion of folic acid to pteric acid. *J. Org. Chem.* **1981**, *46*, 3666–3667.

(31) Bouchoucha, M.; Jaber, M.; Onfroy, T.; Lambert, J.-F.; Xue, B. Glutamic Acid Adsorption and Transformations on Silica. *J. Phys. Chem. C* **2011**, *115*, 21813–21825.

(32) Sebben, D.; Pendleton, P. Analysis of ionic strength effects on the adsorption of simple amino acids. *J. Colloid Interface Sci.* **2015**, *443*, 153–161.

(33) Neuberger, A. Dissociation constants and structures of glutamic acid and its esters. *Biochem. J.* **1936**, *30*, 2085–2094.

(34) Szakács, Z.; Noszál, B. Determination of dissociation constants of folic acid, methotrexate, and other photolabile pteridines by pressure-assisted capillary electrophoresis. *Electrophoresis* **2006**, *27*, 3399–3409.

(35) Federiconi, F.; Mattioni, M.; Baldassarri, E. J.; Ortore, M. G.; Mariani, P. How soft are biological helices? A measure of axial and lateral force constants in folate quadruplexes by high-pressure X-ray diffraction. *Eur. Biophys. J.* **2011**, *40*, 1225–1235.

(36) Kahlweit, M. Ostwald ripening of precipitates. *Adv. Colloid Interface Sci.* **1975**, *5*, 1–35.

(37) Rouw, P. W.; Woutersen, A. T. J. M.; Ackerson, B. J.; De Kruif, C. G. Adhesive hard sphere dispersions: V. Observation of spinodal decomposition in a colloidal dispersion. *Phys. A* **1989**, *156*, 876–898.

(38) Penders, M. H. G. M.; Vrij, A. Spinodal decomposition in a sterically stabilized colloidal silica dispersion following from quench experiments. *Adv. Colloid Interface Sci.* **1991**, *36*, 185–217.

(39) Brinker, C. J.; Scherer, G. W. *Film Formation Sol-Gel Science*; Academic Press: San Diego, 1990; Chapter 13, pp 786–837.

(40) Uhlmann, D. R.; Suratwala, T.; Davidson, K.; Boulton, J. M.; Teowee, G. Sol-gel derived coatings on glass. *J. Non-Cryst. Solids* **1997**, *218*, 113–122.

(41) Lipski, A. M.; Jaquiere, C.; Choi, H.; Eberli, D.; Stevens, M.; Martin, I.; Chen, I.-W.; Shastri, V. P. Nanoscale Engineering of Biomaterial Surfaces. *Adv. Mater.* **2007**, *19*, 553–557.

(42) Malara, N.; Coluccio, M. L.; Limongi, T.; Asande, M.; Trunzo, V.; Cojoc, G.; Raso, C.; Candeloro, P.; Perozziello, G.; Raimondo, R.; De Vitis, S.; Roveda, L.; Renne, M.; Prati, U.; Mollace, V.; Di Fabrizio, E. Folic Acid Functionalized Surface Highlights 5-Methylcytosine-Genomic Content within Circulating Tumor Cells. *Small* **2014**, *10*, 4324–4331.

(43) Zhang, S.; Bai, H.; Luo, J.; Yang, P.; Cai, J. A recyclable chitosan-based QCM biosensor for sensitive and selective detection of breast cancer cells in real time. *Analyst* **2014**, *139*, 6259–6265.

(44) Yin, F.; Zhang, B.; Zeng, S.; Lin, G.; Tian, J.; Yang, C.; Wang, K.; Xu, G.; Yong, K.-T. Folic acid-conjugated organically modified silica nanoparticles for enhanced targeted delivery in cancer cells and tumor in vivo. *J. Mater. Chem. B* **2015**, *3*, 6081–6093.

(45) Henne, W. A.; Doorneweerd, D. D.; Lee, J.; Low, P. S.; Savran, C. Detection of Folate Binding Protein with Enhanced Sensitivity Using a Functionalized Quartz Crystal Microbalance Sensor. *Anal. Chem.* **2006**, *78*, 4880–4884.

(46) Blodgett, K. B. Films Built by Depositing Successive Monomolecular Layers on a Solid Surface. *J. Am. Chem. Soc.* **1935**, *57*, 1007–1022.

(47) Kamikawa, Y.; Nishii, M.; Kato, T. Self-Assembly of Folic Acid Derivatives: Induction of Supramolecular Chirality by Hierarchical Chiral Structures. *Chem.—Eur. J.* **2004**, *10*, 5942–5951.

(48) Kanie, K.; Yasuda, T.; Kato, T.; Ujiie, S. Thermotropic liquid-crystalline folic acid derivatives: supramolecular discotic and smectic aggregation. *Chem. Commun.* **2000**, 1899–1900.

(49) Pinnavaia, T. J.; Marshall, C. L.; Mettler, C. M.; Fisk, C. L.; Miles, H. T.; Beckefr, E. D. Alkali metal ion specificity in the solution ordering of a nucleotide, 5'-guanosine monophosphate. *J. Am. Chem. Soc.* **1978**, *100*, 3625–3627.